

Bilayer-templated two-dimensional RAFT polymerization for directed assembly of polymer nanostructures

Sergey A. Dergunov* and Eugene Pinkhassik*

Abstract: Co-localization of monomers, crosslinkers, and chain-transfer agents (CTA) within self-assembled bilayers in an aqueous suspension enabled the successful directed assembly of nanocapsules using a reversible addition-fragmentation chain transfer (RAFT) process without compromising the polymerization kinetics. This study uncovered substantial influence of the organized medium on the course of the reaction, including differential reactivity based on placement and mobility of monomers, crosslinkers, and CTAs within the bilayer.

This study investigates the application of RAFT polymerization in the confines of a self-assembled bilayer as a means of directed assembly of polymer nanostructures. Among modern controlled/living radical polymerization methods, RAFT has emerged as a promising technique due to its versatility and simplicity and because the polymer is free from the contamination of metal catalysts.^[1-2] It was recently used to produce polymer nanostructures with different shapes.^[3-13] A common drawback of “living” free radical polymerization methods includes slow reaction rates in bulk solution due to the need to keep the concentration of radicals relatively low compared to the concentration of a mediating agent (for example, RAFT or degenerative chain transfer) in order to limit the biradical termination. Herein we investigate the RAFT polymerization within the hydrophobic interior of a bilayer, essentially a two-dimensional solvent, to produce nanostructures replicating the shape of the bilayer morphology without compromising the polymerization kinetics.

In the past, we and others used the free-radical polymerization of hydrophobic monomers in the hydrophobic interior of different assemblies of amphiphilic molecules to produce nanocapsules,^[14-23] nanodisks,^[24-28] and nanorods.^[29-30] Nanocapsules, having an average diameter programmed between 40 to 400 nm with narrow size distribution and the ability to entrap and retain molecules and nanoparticles,^[31-35] showed utility in diverse applications, such as nanoreactors,^[33, 36-37] nanosensors,^[16, 25, 38-41] or containers for the delivery of drugs and imaging agents.^[42-43] The formation of hollow vesicle-templated nanocapsules and the ability to imprint programmed nanopores was demonstrated by a combination of electron microscopy, dye retention, and scattering techniques.^[15-17, 19, 39, 44] The uniform single-nanometer thickness of the shells was confirmed by small-angle neutron scattering.^[31-32] Controlled permeability of nanocapsules was crucial in the assembly of hierarchical nanostructures and functional nanodevices.^{[23, 33, 37,}

45-46] These recent studies highlighted the need for integrating synthetic techniques capable of greater structural control in the directed assembly polymer nanomaterials as well as for better understanding of the polymerization within organized self-assembled scaffolds. RAFT appears promising as a synthetic method due to its fine control of the length of polymer chains. Furthermore, restricted growth of the polymer chains makes RAFT suitable for elucidating factors influencing the polymerization in organized media.

Our main goal was to test the hypothesis that RAFT polymerization within the bilayer would not adversely affect the reaction rate and would produce bilayer-templated nanostructures in an aqueous suspension (Figure 1). To gain better understanding of the polymerization within the bilayers, we investigated questions about the effect of the addition of chain-transfer agent (CTA) and its structure on the ability to form a polymer network, as well as the effect of monomer structures on the polymerization in the presence of CTA.

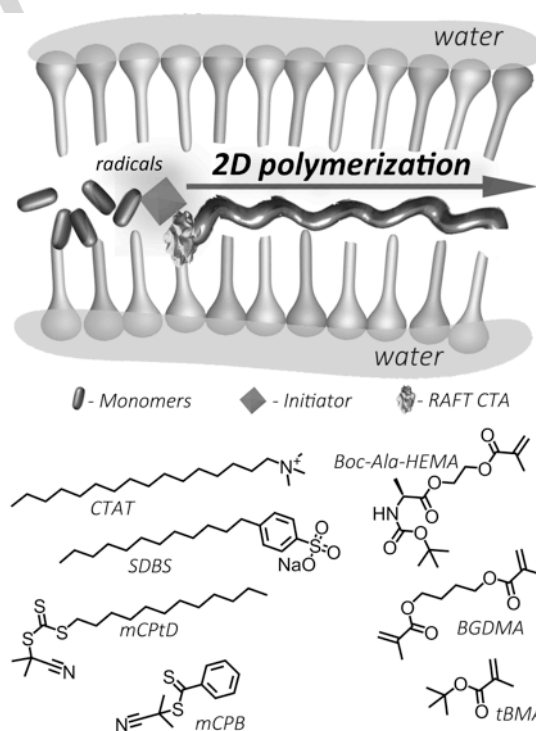


Figure 1. A schematic description of RAFT polymerization of confined monomers within the bilayer of spontaneously assembled vesicles in aqueous solution along with the structures of surfactants, monomers, crosslinkers, and chain-transfer agents.

[*] Dr. S.A. Dergunov, Prof. E. Pinkhassik
Department of Chemistry, University of Connecticut,
55 North Eagleville Road, Storrs, 06269, CT, USA.
E-mail: eugene.pinkhassik@uconn.edu, sergey.dergunov@uconn.edu

Supporting information for this article is given via a link at the end of the document.

We investigated these questions with vesicle-templated RAFT polymerization of amino acid-based methacrylates (Figure S1)^[14, 47-48] using 2-cyano-2-propyl benzodithioate (mCPB) and 2-cyano-2-propyl dodecyl trithiocarbonate (mCPtD) CTAs. These

CTAs were previously used to control the synthesis of methacrylamide and methacrylate homopolymers.^[49-51] We expected them to be located within the bilayer due to their hydrophobic structure while exhibiting different mobility within the bilayer due to their different sizes. In particular, the long hydrophobic tail of the mCPTD (Figure 1) is similar in structure to the surfactants forming the bilayer and can be aligned along with hydrophobic alkyl chains with the active part located in the interstitial layer. In contrast, smaller mCPB molecules (Figure 1) are likely to move more freely within the bilayer. The choice of monomers and crosslinkers was driven by the projected future applications of nanocapsules as biocompatible and biodegradable nanocontainers as well as the motivation to uncover the mobility/reactivity relationships in the organized medium. 2,2'-Azobis(isobutyronitrile) (AIBN) was used as an initiator because of its hydrophobicity and long half-life under the polymerization condition investigated here.

Although one might envision some conceptual similarities between vesicle-templated and emulsion polymerizations, there are two important distinctions. The confinement of monomers ensures the two-dimensional propagation of the growing polymer chains, and vesicles show high longitudinal stability in the timescale of the polymerization, unlike microemulsions.^[52-55]

To assess the association of monomers with the bilayers, we examined ¹H NMR spectra of monomer-loaded vesicles in D₂O. Representative data are shown in Figure 2 with full details presented in Supporting Information. Signals from geminal vinyl protons appeared as two individual peaks in CDCl₃ (Figure 2A). These signals bifurcated when monomers were incorporated in the bilayer (Figure 2A). For example, for Boc-Ala-HEMA each new signal showed a downfield and upfield components (Figure 2A). The chemical shift of the downfield component was nearly identical to the chemical shift of the original signal in CDCl₃. In contrast, the free monomer revealed the trend toward increasing the chemical shift of this hydrogen upon increasing polarity of the solvent from chloroform to methanol (Figure S1). The multiplicity of the signals (a doublet of quartets) was evident for some of the signals in CDCl₃ but was not resolved in vesicle suspensions in D₂O due to signal broadening (Figures 2B and S4). The upfield component revealed substantially greater broadening than the downfield components. We attribute these findings to the differential orientation of the monomers within the bilayer. Broader upfield signals correspond to vinyl protons oriented toward the inner part of the bilayer as well as monomers that are phase-separated in the interstitial layer.

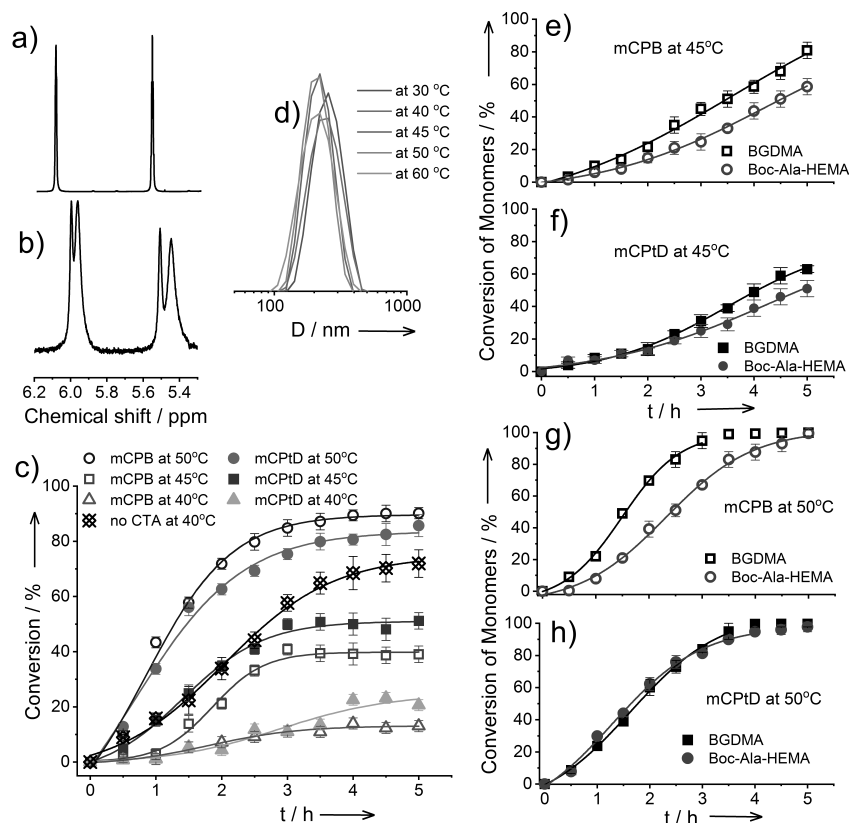


Figure 2. ¹H NMR spectra of Boc-Ala-HEMA monomer in (a) CDCl₃ and (b) synergistically assembled vesicles with the monomer in D₂O. (c) Total conversion-time plots for vesicle-templated RAFT-polymerization of Boc-Ala-HEMA/BGDMA pair at 40 °C (Δ, ▲, ◊), 45 °C (□, ■), 50 °C (○, ●), without (◇) and with mCPB (open figures) and mCPTD (closed figures) chain transfer agents determined by ¹H NMR method. (d) Dependence of size distribution of synergistically assembled vesicles with monomers on temperature. (e-h) Conversion-time plots for vesicle-templated RAFT-polymerization of Boc-Ala-HEMA/BGDMA pair at 45 and 50 °C with mCPB (open figures) and mCPTD (closed figures) chain transfer agents determined by GC-MS method. The lines are guides to the eye only.

Sharper downfield signals belong to vinyl groups associated with the outer portions of the bilayer. This interpretation of the NMR signals is in line with previously reported analysis of the NMR spectra of bilayer-bound molecules.^[14, 56-57] It is also supported by our previous study of the distribution of monomers in the bilayer based on small-angle neutron and X-ray scattering.^[58] Specific ratios of the differential locations of monomers appear to depend on the mobility and hydrophobicity of the monomers^[59] and their ability to form intra- and intermolecular complexes within the bilayer. For example, for styrene-based monomers, half of them were distributed in a bilayer and half were in the interstitial layer (Figures S4d, S4e). However, in the case of methacrylate monomers, the entire amount of monomers was distributed in a bilayer (Figure S4).

We measured total conversions as a function of time for the polymerization of a Boc-Ala-HEMA/BGDMA pair with and without RAFT agents (Figure 2C) to evaluate factors influencing the polymerization in the bilayers. These data were obtained from in-situ ¹H NMR analysis of the monomer-loaded vesicles during the polymerization. The values for conversion are based on the total integration of vinyl hydrogens. Polymerization within the bilayer in the absence of RAFT agents at 40°C was completed in 3 hours with good conversion (60%). Under these conditions, in the presence of RAFT agents, a noticeable drop in the reaction rate was observed. Previously, a similar decrease in the reaction rate was noted during bulk or microemulsion RAFT polymerization of styrenes and methacrylates.^[52, 60-63]

Dynamic light scattering (DLS) data revealed virtually no difference in the size and size distribution of monomer-loaded vesicles at different temperatures (Figure 2D). These observations suggest that the differences in the reaction kinetics discussed in more detail below are not likely to be influenced by the morphology of the aggregates or the curvature of the bilayer but rather by the location and mobility of monomers, crosslinkers, and CTAs.

At higher temperatures, kinetic studies (Figure 2C) confirm fast RAFT copolymerization of Boc-Ala-HEMA and BGDMA within a bilayer; for example, 70% conversion can be achieved within 2 hours at 50 °C for the mCPB CTA (60% for mCPTD). After 5 hours, the same composition leads to a nearly complete (> 90%) conversion of monomers. The formation of a cross-linked polymer network begins as soon as within 30 minutes of reaction for both agents, as shown in electron microscopy studies discussed below, with a high polymer yield after 2 hours of polymerization. With a decrease in polymerization temperatures (40 and 45°C), the formation of a cross-linked polymer occurred only after 2-4 hours of reaction. It is likely that different plateau values for the conversion of monomers observed at different temperatures reflect their differential mobility within the bilayer. It is reasonable to expect that the polymerization would propagate predominantly within the interstitial layer. At lower temperatures, monomers with the vinyl groups positioned away from the interstitial layer may not participate in the formation of the polymer network. Increasing the temperature would lead to an increased proportion of the monomers approaching the growing chain in the timescale of the reaction resulting in a greater proportion of molecules included

in the polymer shell. Likewise, differential apparent reactivities of transfer reagents at different temperatures likely reflect their distribution and mobility within the bilayer. Thus, mCPTD is expected to be aligned along the hydrophobic alkyl sites with active parts located in the interstitial layer and showing lower mobility than mCPB, a smaller molecule. It results in faster reactions and higher yields than mCPB at lower temperatures. In contrast, mCPB shows a higher overall yield at 50°C, likely, due to its higher mobility in the bilayer and the ability to involve a larger number of monomer molecules at higher temperatures.

To gain further insights into the differential reactivity within the bilayer, we performed a series of kinetic experiments using GC-MS to monitor the concentration of each building block (Figure 2E-H). In particular, we were interested in the differential reactivity of the monomer and crosslinker under the polymerization conditions. NMR and GC-MS methods provide complementary data since NMR reveals vinyl groups of crosslinkers incorporated into oligomers while GC-MS only shows unreacted molecules. The differential reactivity appeared to depend on the RAFT agents and temperature. At 45 °C, the crosslinker disappeared faster from the solution when mCPB was used (Figure 2E) while the difference was less pronounced for mCPTD (Figure 2F). At 50°C, the contrast was more dramatic, revealing a substantial difference in reactivity with mCPB (Figure 2G) and no measurable difference with mCPTD (Figure 2H). For example, at the 2.5 hrs. point, less than 50% of monomer and more than 85% of crosslinker reacted when mCPB was used. With mCPTD, both monomer and crosslinker showed an 80% conversion at the same time. These findings support the influence of the organized medium and the interplay between the localization and mobility of monomers, crosslinkers, and RAFT agents in the outcome of the polymerization. More hydrophobic amino acid-based methacrylate monomers, such as Boc-Phe-HEMA or Boc-Pro-HEMA,^[59, 64] show comparable results (see Supporting Information). On the other hand, when using more mobile systems with smaller hydrophobic monomers, such as tBMA/BGDMA or tBMA/DVB pairs, the monomers in these pairs react faster and completely disappear at the initial stages of polymerization (Figure S7). While Boc-Ala-HEMA is comparable in size to BGDMA, tBMA is much smaller and is expected to reveal higher mobility within the bilayer. For example, at 40°C, nearly 100% of tBMA is consumed within 2.5 hours while roughly 8% of BGDMA reacted (Figure S7b). The inherent reactivity of the acrylic moiety should be the same; therefore, the difference in reactivity is likely to stem from mobility. One could match the reactivity of different building blocks by adjusting the reaction temperature, e.g., the conversion of BGDMA at 2.5 hours was roughly 40% at 45° C (Figure S7d) and more than 85% at 50°C (Figure S7g).

We investigated the size of linear polymer chains formed within the bilayer in the absence of crosslinkers with gel permeation chromatography (GPC) to validate the expectation of controlled chain growth under RAFT polymerization. Without CTAs, free-radical polymerization (5h, 40 °C) resulted in average molecular weight exceeding 400kDa (Figure S8). In contrast, RAFT polymerization (5h, 45 °C) produced chains with an average molecular weight around 40kDa (Figure S8). In a

series of control experiments, polymerization was performed in the presence of CTAs and under UV irradiation. The results showed a broad distribution of products indicative of the competition between RAFT and UV-induced free-radical polymerization (Figures S9 and S10). Low dispersity index (<1.4) for products of RAFT polymerization confirmed the ability to control the chain growth in two-dimensional medium. This outcome sets the stage for the rational design of nanomaterials for targeted applications, e.g., biodegradable nanocontainers with small, readily excretable fragments.

Next, we applied bilayer-confined RAFT polymerization to the synthesis of nanocapsules. After 5 hours, all compositions lead to almost complete ($> 90\%$) conversion of monomers and produced nanocapsules with an average diameter of about 200 nm, characterized by dynamic light scattering (DLS) and SEM. DLS data show that the diameter of the nanocapsules closely matches the diameter of parent templating vesicles (Supporting Information). The formation of hollow nanocapsules was supported by benchmark control experiments performed in a similar fashion to the previous reports and detailed in the Supporting Information (Figures S11, S12, S13, Table S1). Figure 3 shows an example of transmission electron microscopy (TEM) images of newly prepared nanocapsules.

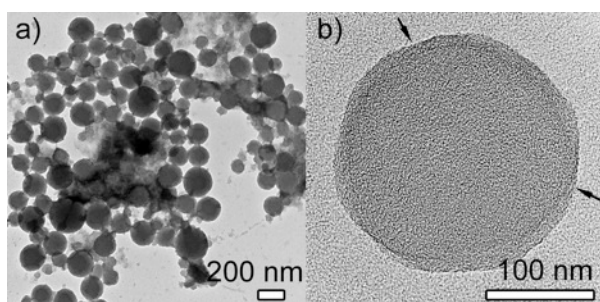


Figure 3. (a) TEM images of hollow nanocapsules produced using the mCPTD transfer agent after 5 hours of polymerization. Boc-Ala-HEMA / BGDMA based nanocapsules synthesized at 45°C and after synthesis precipitated with methanol, washed thoroughly with methanol and water. (b) High resolution TEM image of a nanocapsule with well-defined boundaries.

We used entrapment assays to evaluate the integrity of the shells of nanocapsules formed by the new RAFT initiation method. In these experiments, we created nanocapsules in the presence of molecules with different smallest dimensions, acting as size probes (Figure 4). After polymerization and removal of the surfactant scaffold, we washed nanocapsules until the supernatant became colorless to remove any molecules that escaped from the capsule interior. Molecules smaller than the pore size escape from the capsules, while molecules larger than the pore size remain entrapped.^[17] High rates of mass transfer through the pores due to single-nanometer thickness of the shells ensure that complete removal of small molecules occurs in the timescale of the handling of nanocapsules in these experiments.^[16, 36, 38] Capsules with pinhole defects exceeding the size probes will not be able to retain the encapsulated molecules due to the rapid efflux of molecules smaller than the

pore size. We used Nile Blue A and Doxorubicin as small and midsize probes, which are representative of a broad range of cargo molecules, such as drugs for targeted delivery. With a reaction time of more than 3 hours for both probes, as well as for both RAFT agents, intensely colored nanocapsules were obtained with no extraneous structures (Figures 4, 5), which indicates the high-yield formation of fully formed polymer structures with no pinhole defects. At short reaction times, small molecules were either not retained or retained in the amounts much smaller than entrapped in the aqueous core of templating vesicles (Figures 4, S14a).

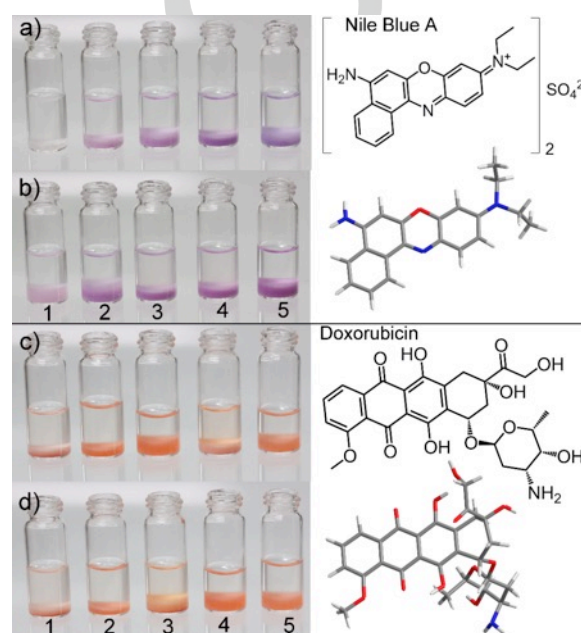


Figure 4. Photographs of the corresponding samples of nanocapsules containing entrapped small (Nile Blue A, with smaller size about 0.9 nm) and midsize (Doxorubicin, with smaller size about 1.6 nm) dyes in methanol after 1, 2, 3, 4 and 5 hours of polymerization. Nanocapsules polymerized using mCPTD (a and c) and mCPTD (b and d) transfer agent.

Scanning electron microscopy (SEM) data showed that even after 30 minutes of reaction, the formation of cross-linked polymers occurs, although the final product does not have a spherical architecture and is present only in the form of an amorphous polymer structure for both systems of chain transfer agents (Figure 5a and 5e). In addition, the GPC analysis of the solutions collected after the precipitation of nanocapsules showed only the presence of surfactants and unreacted monomers, and the absence of traces of the formation of soluble homopolymers, which may indicate the similarity of the copolymerization kinetics under these conditions, and the formation of mainly cross-linked structures throughout the polymerization. After 1 hour of the reaction, the formation of spherical structures began with more pronounced structures in the case of mCPTD (Figure 5b and 5f). After 3 hours of polymerization, only nanocapsules are predominant for both systems (Figure 5c, 5d, 5g, and 5h). Coupled with dye retention

data (Figure 4), SEM results suggest that at early stages of polymerization, crosslinked structures are formed in the bilayer with spherical structures likely containing holes large enough for dyes to escape but too small to be observed in SEM. At later stages of polymerization, the reaction produces a high yield of nanocapsules with no extraneous structures.

Control experiments performed at high temperature or high concentration of vesicles leading to vesicle instability resulted in the formation of micron-sized spherical structures indicative of the collapse of vesicles into microemulsions (Figures S14b, S14c). At low vesicle concentrations, the kinetics of the polymerization was the same as shown on Figure 2 when expressed as percent conversion of monomers (Figure S14d), suggesting that each vesicle acts as an isolated reaction vessel acting independently of other vesicles in the suspension.

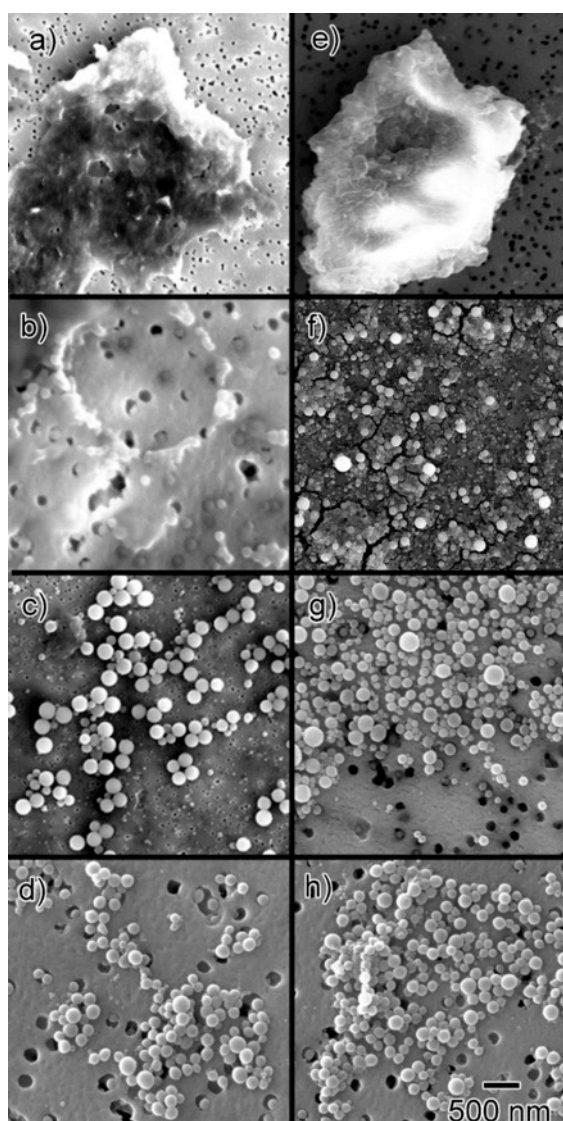


Figure 5. SEM images obtained for amino acid-based nanocapsules polymerized using mCPB (a-d) and mCPtD (e-h) transfer agent after 30 min (a, e), 1 h (b, f), 3 h (c, g) and 5 h (d, h) of polymerization.

Deprotected nanocapsules were characterized by zeta potential measurements (Figure 6). At the initial stage of conversion (below 30%), the surface charge (Figure 6a) was screened due to the lower reactivity of Boc-Ala-Hema compared to BGDMA. After 35–40% of the conversion, only strongly cationic particles were formed. The data between 70% and 90% conversion highlight the differential reactivity described in Figure 2. Due to lower reactivity of monomers with mCPB, corresponding capsules have a lower concentration of ionic groups on the surface and reveal lower zeta potential at the same conversion values than capsules produced with mCPtD (Figure 6a).

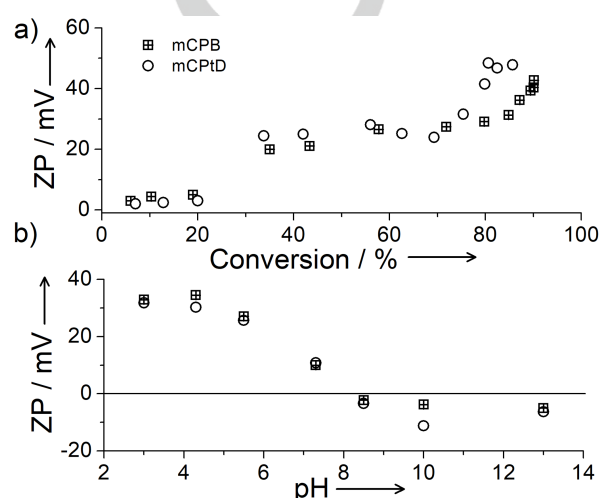


Figure 6. Zeta potential obtained for aqueous dispersions of deprotected amino acid-based nanocapsules polymerized using mCPB and mCPtD CTAs. a) Zeta potential vs. conversion of monomers, b) zeta potential vs. pH.

The pH-dependent zeta potential values were measured for fully formed nanocapsules at the final stage of polymerization (Figure 6b). As expected, amino groups in polymer nanocapsules led to high cationic zeta potentials in acidic conditions due to complete protonation, while basic conditions resulted in nearly zero zeta potential values indicative of lack of ionization. The nanocapsules obtained with both CTAs showed similar electrophoretic behavior depending on the pH of the solution, which indicates similar polymerization parameters and the formation of equivalent amounts of charged groups on the surface of the nanocapsules.

In summary, we have demonstrated the successful implementation of RAFT polymerization in an organized medium of self-assembled bilayers. This method is a viable approach to the directed assembly of functional nanomaterials as confirmed by the successful assembly of nanocapsules. Unlike slow polymerization in the bulk, the kinetics of RAFT polymerization observed here matches the expectations for a two-dimensional solvent. The kinetic data observed at different temperatures and with different CTAs coupled with the NMR data supporting differential orientation and distribution of monomers within the bilayer point toward a more complex interplay between the

organized environment of the scaffold and the building blocks being assembled into a well-defined nanostructure compared with reactions in bulk or non-organized media. Furthermore, adjustments in reaction conditions, including the structure of building blocks and CTAs and reaction temperature proved to be successful in producing nanostructures with desired characteristics. Previously reported synergistic co-assembly of scaffolds and building blocks is likely to be a particularly fruitful avenue for pursuing the creation of nanoarchitectures with high precision.^[65] The application of controlled polymerization methods, such as RAFT, will be an essential element in understanding and controlling the assembly of building blocks within organized self-assembled scaffolds.

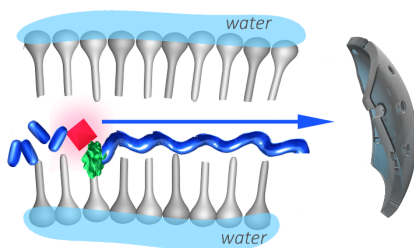
Acknowledgments

This work was supported by the National Science Foundation (CHE-1709921) and the University of Connecticut Research Excellence Program. SEM characterization was performed using the facilities in the UConn/FEI Center for Advanced Microscopy and Materials Analysis (CAMMA).

Keywords: nanocapsules • RAFT-polymerization • organized media

- [1] A. Goto, T. Fukuda, *Prog. Polym. Sci.* **2004**, *29*, 329-385.
- [2] B. Ochiali, T. Endo, *Prog. Polym. Sci.* **2005**, *30*, 183-215.
- [3] Y. Wang, S. Dadashi-Silab, K. Matyjaszewski, *ACS Macro Letters* **2018**, *7*, 720-725.
- [4] N. P. Truong, C. Zhang, T. A. H. Nguyen, A. Anastasaki, M. W. Schulze, J. F. Quinn, A. K. Whittaker, C. J. Hawker, M. R. Whittaker, T. P. Davis, *ACS Macro Letters* **2018**, *7*, 159-165.
- [5] H. Zhou, C. Liu, Y. Qu, C. Gao, K. Shi, W. Zhang, *Macromolecules* **2016**, *49*, 8167-8176.
- [6] J. Lesage de la Haye, X. Zhang, I. Chaduc, F. Brunel, M. Lansalot, F. D'Agosto, *Angew. Chem. Int. Ed.* **2016**, *55*, 3739-3743.
- [7] K. Min, H. Gao, K. Matyjaszewski, *J. Am. Chem. Soc.* **2006**, *128*, 10521-10526.
- [8] M. Semsarilar, V. Ladmiraal, A. Blanazs, S. P. Armes, *Langmuir* **2012**, *28*, 914-922.
- [9] W. Zhang, F. D'Agosto, O. Boyron, J. Rieger, B. Charleux, *Macromolecules* **2011**, *44*, 7584-7593.
- [10] W. Zhang, F. D'Agosto, O. Boyron, J. Rieger, B. Charleux, *Macromolecules* **2012**, *45*, 4075-4084.
- [11] P. Gurnani, A. B. Cook, R. A. E. Richardson, S. Perrier, *Polym Chem* **2019**, *10*, 1452-1459.
- [12] P. Gurnani, C. Sanchez-Cano, K. Abraham, H. Xandri-Monje, A. B. Cook, M. Hartlieb, F. Lévi, R. Dallmann, S. Perrier, *Macromolecular Bioscience* **2018**, *18*, 1800213.
- [13] S. I. Ali, J. P. A. Heuts, A. M. van Herk, *Langmuir* **2010**, *26*, 7848-7858.
- [14] S. A. Dergunov, *ACS Macro Letters* **2018**, *7*, 1322-1327.
- [15] S. A. Dergunov, K. Kesterson, W. Li, Z. Wang, E. Pinkhassik, *Macromolecules* **2010**, *43*, 7785-7792.
- [16] S. A. Dergunov, B. Miksa, B. Ganus, E. Lindner, E. Pinkhassik, *Chem. Commun.* **2010**, *46*, 1485-1487.
- [17] S. A. Dergunov, E. Pinkhassik, *Angew. Chem. Int. Ed.* **2008**, *47*, 8264-8267.
- [18] M. D. Kim, S. A. Dergunov, E. Pinkhassik, *Langmuir* **2015**, *31*, 2561-2568.
- [19] M. D. Kim, S. A. Dergunov, A. G. Richter, J. Durbin, S. N. Shmakov, Y. Jia, S. Kenbeilova, Y. Orazbekuly, A. Kengpeil, E. Lindner, S. V. Pingali, V. S. Urban, S. Weigand, E. Pinkhassik, *Langmuir* **2014**, *30*, 7061-7069.
- [20] D. H. W. Hubert, M. Jung, A. L. German, *Adv. Mater.* **2000**, *12*, 1291-1294.
- [21] J. Kurja, R. J. M. Nolte, I. A. Maxwell, A. L. German, *Polymer* **1993**, *34*, 2045-2049.
- [22] J. Murtagh, J. K. Thomas, *Faraday Discuss. Chem. Soc.* **1986**, *81*, 127-136.
- [23] S. A. Dergunov, M. D. Kim, S. N. Shmakov, E. Pinkhassik, *Acc. Chem. Res.* **2019**, *52*, 189-198.
- [24] S. Tekobo, A. Richter, S. A. Dergunov, S. Pingali, V. Urban, B. Yan, E. Pinkhassik, *J. Nanopart. Res.* **2011**, *13*, 6427-6437.
- [25] Y. Zhang, S. Tekobo, Y. Tu, Q. Zhou, X. Jin, S. A. Dergunov, E. Pinkhassik, B. Yan, *ACS Appl. Mater. Interfaces* **2012**, *4*, 4099-4105.
- [26] S. C. L. Hall, C. Tognoloni, G. J. Price, B. Klumperman, K. J. Edler, T. R. Dafforn, T. Arnold, *Biomacromolecules* **2018**, *19*, 761-772.
- [27] K. Yasuhara, J. Arakida, T. Ravula, S. K. Ramadugu, B. Sahoo, J.-i. Kikuchi, A. Ramamoorthy, *J. Am. Chem. Soc.* **2017**, *139*, 18657-18663.
- [28] A. O. Oluwole, J. Klingler, B. Danielczak, J. O. Babalola, C. Vargas, G. Pabst, S. Keller, *Langmuir* **2017**, *33*, 14378-14388.
- [29] D. Pati, S. Das, N. G. Patil, N. Parekh, D. H. Anjum, V. Dhaware, A. V. Ambade, S. Sen Gupta, *Biomacromolecules* **2016**, *17*, 466-475.
- [30] S. Shin, S. H. Gihm, C. R. Park, S. Kim, S. Y. Park, *Chem. Mater.* **2013**, *25*, 3288-3295.
- [31] S. A. Dergunov, A. G. Richter, M. D. Kim, S. V. Pingali, V. S. Urban, E. Pinkhassik, *Langmuir* **2019**, *35*, 13020-13030.
- [32] A. G. Richter, S. A. Dergunov, M. D. Kim, S. N. Shmakov, S. V. Pingali, V. S. Urban, Y. Liu, E. Pinkhassik, *J. Phys. Chem. Lett.* **2017**, *8*, 3630-3636.
- [33] S. N. Shmakov, Y. Jia, E. Pinkhassik, *Chem. Mater.* **2014**, *26*, 1126-1132.
- [34] M. D. Kim, S. A. Dergunov, E. Pinkhassik, *Langmuir* **2017**, *33*, 7732-7740.
- [35] S. N. Shmakov, E. Pinkhassik, *Chem. Commun.* **2010**, *46*, 7346-7348.
- [36] S. A. Dergunov, A. T. Khabyev, S. N. Shmakov, M. D. Kim, N. Ehterami, M. C. Weiss, V. B. Birman, E. Pinkhassik, *ACS Nano* **2016**, *10*, 11397-11406.
- [37] Y. Jia, S. N. Shmakov, P. Register, E. Pinkhassik, *Chem. Eur. J.* **2015**, *21*, 12709-12714.
- [38] M. D. Kim, S. A. Dergunov, E. Lindner, E. Pinkhassik, *Anal. Chem.* **2012**, *84*, 2695-2701.
- [39] S. A. Dergunov, M. D. Kim, S. N. Shmakov, A. G. Richter, S. Weigand, E. Pinkhassik, *Chem. Eur. J.* **2016**, *22*, 7702-7705.
- [40] A. Q. Maclin, M. D. Kim, S. A. Dergunov, E. Pinkhassik, E. Lindner, *Electroanalysis* **2015**, *27*, 733-744.
- [41] Y. Jia, S. N. Shmakov, E. Pinkhassik, *ACS Appl. Mater. Interfaces* **2016**, *8*, 19755-19763.
- [42] S. A. Dergunov, J. Durbin, S. Pattanaik, E. Pinkhassik, *J. Am. Chem. Soc.* **2014**, *136*, 2212-2215.
- [43] S. A. Dergunov, E. Pinkhassik, *J. Am. Chem. Soc.* **2011**, *133*, 19656-19659.
- [44] D. C. Danila, L. T. Banner, E. J. Karimova, L. Tsurkan, X. Y. Wang, E. Pinkhassik, *Angew. Chem. Int. Ed.* **2008**, *47*, 7036-7039.
- [45] S. N. Shmakov, S. A. Dergunov, E. Pinkhassik, *Chem. Commun.* **2011**, *47*, 8223-8225.
- [46] S. A. Dergunov, N. Ehterami, E. Pinkhassik, *Chem. Eur. J.* **2016**, *22*, 14137-14140.
- [47] S. Kumar, S. G. Roy, P. De, *Polym. Chem.* **2012**, *3*, 1239-1248.
- [48] H. Sun, C. Gao, *Biomacromolecules* **2010**, *11*, 3609-3616.
- [49] R. Bleach, B. Karagoz, S. M. Prakash, T. P. Davis, C. Boyer, *ACS Macro Letters* **2014**, *3*, 591-596.
- [50] M. Le Neindre, B. Magny, R. Nicolaÿ, *Polym Chem* **2013**, *4*, 5577-5584.
- [51] Y. Kametani, M. Sawamoto, M. Ouchi, *Angew. Chem. Int. Ed.* **2018**, *57*, 10905-10909.
- [52] M. J. Monteiro, M. Hodgson, H. D. Brouwer, *J. Polym. Sci., Part A: Polym. Chem.* **2000**, *38*, 3864-3874.
- [53] M. J. Monteiro, M. Sjöberg, J. v. d. Vlist, C. M. Göttgens, *J. Polym. Sci., Part A: Polym. Chem.* **2000**, *38*, 4206-4217.
- [54] Y. Kitayama, S. Tomoeda, M. Okubo, *Macromolecules* **2012**, *45*, 7884-7889.
- [55] H. Maehata, C. Buragina, M. Cunningham, B. Keoshkerian, *Macromolecules* **2007**, *40*, 7126-7131.
- [56] W.-g. Wu, S.-W. Leu, C.-H. Hsieh, L.-M. Chi, *Chem. Phys. Lipids* **1991**, *58*, 241-248.
- [57] G. L. Jendrasiak, R. Smith, A. A. Ribeiro, *Biochim. Biophys. Acta* **1993**, *1145*, 25-32.
- [58] A. G. Richter, S. A. Dergunov, B. Ganus, Z. Thomas, S. V. Pingali, V. Urban, Y. Liu, L. Porcar, E. Pinkhassik, *Langmuir* **2011**, *27*, 3792-3797.
- [59] W. C. Wimley, S. H. White, *Nat. Struct. Mol. Biol.* **1996**, *3*, 842-848.
- [60] S. Liu, K. D. Hermanson, E. W. Kaler, *Macromolecules* **2006**, *39*, 4345-4350.
- [61] R. Plummer, Y.-K. Goh, A. K. Whittaker, M. J. Monteiro, *Macromolecules* **2005**, *38*, 5352-5355.
- [62] M. J. Monteiro, H. de Brouwer, *Macromolecules* **2001**, *34*, 349-352.
- [63] M. J. Monteiro, *J. Polym. Sci., Part A: Polym. Chem.* **2005**, *43*, 3189-3204.
- [64] J. Kyte, R. F. Doolittle, *J. Mol. Biol.* **1982**, *157*, 105-132.
- [65] S. A. Dergunov, A. G. Richter, M. D. Kim, S. V. Pingali, V. S. Urban, E. Pinkhassik, *Chem. Commun.* **2013**, *49*, 11026-11028.

Text for Table of Contents



Sergey A. Dergunov* and Eugene
Pinkhassik*

Page No. – Page No.

**Bilayer-templated two-dimensional
RAFT polymerization for directed
assembly of polymer nanostructures**

WILEY-VCH